Title: *Admp* regulates tail bending by controlling ventral epidermal cell polarity via phosphorylated myosin translocation (115/120 char.)

Yuki S. Kogure [1], Hiromochi Muraoka [1], Wataru C. Koizumi [1], Raphaël Gelin-alessi [1], Benoit Godard [2], C. P. Heisenberg [2], Kotaro Oka [1,3,4] and Kohji Hotta [1]*

Affiliations

[1] Department of Biosciences and Informatics, Faculty of Science and Technology, Keio University, Kouhoku-ku, Yokohama 223-8522, Japan

[2] Institute of Science and Technology Austria, Klosterneuburg, Austria

[3] Waseda Research Institute for Science and Engineering, Waseda University, 2-2 Wakamatsucho, Shinjuku, Tokyo 162-8480, Japan

[4] Graduate Institute of Medicine, College of Medicine, Kaohsiung Medical University, Kaohsiung City 80708, Taiwan

*** Correspondence:** Kohji Hotta**,** khotta@bio.keio.ac.jp

Running Title (32/32): Polarity by *Admp* regulated tail bending

Summary Statement (30/30 words): *Admp* is an upstream regulator of the tail bending in the protochordate *Ciona* tailbud embryo, regulating tissue polarity of the ventral midline epidermis by the translocation of the phosphorylated myosin.

Keywords (3-6): tunicate, tail bending, intercalation, polarity, apical-constriction, embryo shape

Abstract (179/180 words):

The tail's transient but pronounced ventral bending is found in many chordate embryos and provides an interesting model of how tissue interactions contribute to the overall shape (Lu et al., 2020). Here, we identify one of the upstream regulators of tail bending. *Admp* knock-down embryo (*Admp* MO) completely inhibited ventral tail bending. *Admp* MO showed specific inhibition of the cell-cell intercalation ventral epidermis. In the

early stages of the intercalation, each ventral epidermal cell exhibited a boat-shaped morphology (boat cell) with a narrow apical surface in which phosphorylated myosin (pMLC) accumulated. In the *Admp* MO, the number of the boat cells reduced and pMLC was observed at the basal side in the *A*dmp MO embryo. Finally, laser cutter experiments showed a pMLC-dependent relaxation of the ventral tail bending, which was observed when each ventral midline epidermal cell was cut along the apico-basal axis. Based on these results, we propose a novel function for *Admp*, in which Admp controls the pMLC translocation to the apical side of the ventral epidermal cells and leads the tail bending by ventral resistance to the notochord extension.

(main text approx. 6318/7000 words)

Introduction

Although chordates have various shapes and sizes in the adult stage, they have similar shapes during their organogenesis period, called the phylotypic stage (Klaus., 1983). During the phylotypic stage, chordates pass through neurulation and subsequently reach the tailbud stage. At the chordate tailbud stage, the embryo tail elongates along the anterior-posterior (AP) axis, and most tailbud embryos become curved shape (Richardson et al., 1997), bending the tail.

The protochordata, ascidian *Ciona intestinalis* type A (*Ciona robusta*) embryo also shows tail bending ventrally (ventroflexion) in the early- to mid- tailbud stages [stage (st.) 19 to st. 22], and then the bending relaxed and start to bend dorsally (dorsiflexion) in order, even if the egg envelope is removed (Hotta et al., 2007).

This means that *Ciona* tail bending occurs independently without external force (Hotta et al., 2007; Lu et al., 2020).

Because the notochord changes cell shape using circumferential contraction force during st. 21 to 24 (Lu et al., 2019; Mizotani et al., 2018; Sehring et al., 2014), the transverse loading generated by the circumferential constrictive force on a

compression-resisting system is converted into a pushing force that is especially higher along the longitudinal axis (Lu et al., 2019; Miyamoto and Crowther, 1985).

Although it has been shown that a longitudinal pushing force is exerted by each notochord cell (Sehring et al., 2014; Zhou et al., 2015) and the tail elongation has suggested that the notochord actively produces an AP elongating force (Miyamoto and Crowther, 1985; Sehring et al., 2014; Spemann, 1987; Ubisch, 1939), the mechanism of tail bending in the tailbud embryo has been unknown until a recent study by Lu et al. (2020). These authors investigated the internal molecular mechanism that enables *Ciona* to bend its early tailbud and reported that the main factor of the tail bending during the early tailbud stages (st. 18 to st. 20) is the different contraction force by the actomyosin between the ventral and the dorsal sides of the notochord. However, the upstream regulators involved in tail bending and the morphogenetic mechanisms contributing to bending after st. 20 remain unclear.

To identify the upstream regulator of tail bending and investigate the later tail bending mechanism after st. 20 in the *Ciona* tailbud embryos, we performed knock-down experiments, a morphological analysis of tailbud embryo using three-dimensional (3D) imaging, inhibitor treatment, immunostaining, and laser cutting experiments. Here we show that *Admp* regulates cell polarity by translocating phosphorylated myosin (pMLC) in ventral midline epidermal cells, converting it into the mechanical resistance in the AP direction required for proper tail bending in mid-tailbud stages, st. 18 to st. 22.

Results

Admp MO suppressed ventral tail bending but not dorsal tail bending

In some previous studies, *Admp* knock-down by antisense morpholino (*Admp* MO) mutant embryos did not appear to have tail bending in mid-tailbud stages (Imai,

2006; Imai et al., 2012; Pasini et al., 2006). We focused on the *Admp* as one of the candidates for the upstream regulators of the tail bending.

To confirm our hypothesis, we first performed microinjection of the morpholino antisense oligo (MO) and observed the phenotype in a time-lapse movie (Fig.1A, Suppl. Mov. 1). As a result, no bending to ventral (ventroflexion; Fig. 1A, red arrow) was observed at the mid-tailbud stages of the *Admp* MO embryo; afterward, bending to dorsal (dorsiflexion; Fig. 1A, yellow arrows) was observed similar to WT. When the bending angle of *Admp* MO embryos and WT at st. 18 to 22 (in which WT ventroflexion occurs) were compared (Fig. 1B), that of the *Admp* MO embryos was significantly reduced (Fig. 1C; N = 11/11). The tailbud embryos treated with dorsomorphin – an Admp/Bmp signaling inhibitor – also significantly reduced the bending angle (Fig. 1D; N = 5–12, Suppl. Fig. 1A and 1B). Therefore, it was suggested that Admp/BMP specifically regulates the ventroflexion of the ascidian tailbud embryos.

Although a previous study has shown that notochord actomyosin asymmetry is responsible for tail bending during st. 18 to st. 20 (Lu et al., 2020), asymmetric localization of notochord actomyosin in the dorsoventral region was observed even in the *Admp* MO morphant at st. 18 to 22 (Suppl. Fig. 2).

The *Admp* gene is one of the BMP ligands, and in *Ciona*, it has been reported that the *Admp*/*BMP* signal induces the differentiation of ventral peripheral neurons (Imai et al., 2012; Waki et al., 2015) and that *Msxb* is involved in the differentiation of epidermal neurons as a downstream target of *Admp* (Imai et al., 2012). Next, we investigated whether the Admp-downstream target, *Msxb*, also regulates the tail bending. However, even if the *Msxb* has been knocked down, the ventroflexion seems normal (Suppl. Fig. 1C).

Therefore, we hypothesized that *Admp* might control the morphology of tail bending, apart from the downstream pathway of *Msxb* that controls the

differentiation of ventral peripheral neurons (Roure and Darras, 2016; Waki et al., 2015).

Smad phosphorylation in ventral midline epidermal cells

In *Ciona*, *Admp* is expressed in the endoderm and lateral epidermis (Imai et al., 2012). Since *Admp* is a morphogen, it can act at sites far from its original place expression (Imai et al., 2012). In vertebrates, *Admp* is expressed dorsally and moves to the opposite side to specify the ventral fate, and it is difficult to predict the target site from its gene expression pattern. On the other hand, it was known that *Admp* promotes *bmp4* expression and controls the positioning of *bmp4* expression during regeneration of left-right asymmetric fragments in planarian (Gaviño and Reddien, 2011).

In *Ciona*, *Admp* expression appeared normal in *Bmp2/4* morphants, but *Bmp2/4* expression was suppressed in *Admp* morphants (Imai et al., 2012). The Bmp target, Smad, was phosphorylated, and the phosphorylated Smad translocates into the nucleus and activates the target genes (Blitz and Cho, 2009; De Robertis, 2009; Imai et al., 2012). The Smad signal of the ventral epidermal cells disappears in the *Ciona* embryo injected with *Admp* MO at the late gastrula stage (Fig.1E; Waki et al., 2015). To determine when and where the Admp/BMP signal was transmitted, we performed antibody staining of phosphorylated Smad, pSmad1/5/8 (Fig. 1E). As a result, consistent with a previous study (Waki et al., 2015), a pSmad signal was observed at the ventral midline epidermal cells after the late gastrula stage (Fig. 1E), and no specific signal was detected in other areas, including notochord, from gastrula to the initial tailbud period. These results showed that *Admp*/*BMP* signal was transmitted to ventral midline epidermal cells.

Admp regulates the cell-cell intercalation of ventral epidermal cells

Next, we investigated the dorsal and ventral epidermis dynamics from st.18 to 24 (Suppl. Fig. 3). The cell-cell intercalation of ventral epidermal cells was started on st.19 and completed at st. 24. The tail epidermis of the ascidian embryo is finally elongated in the anterior-posterior axis by arranging in a row through the cell-cell intercalation (Suppl. Fig. 3; Hotta et al., 2007). However, during the early phase of the ventral cell-cell intercalation from st. 19 to st. 22 did not promote the AP elongation of the tail (early intercalation), which corresponded to the ventroflexion period (Fig. 1A, red arrow). In the later phase of cell-cell intercalation from st. 22 to st. 24, the tail elongates (late intercalation) (Fig.2AB). From this observation, we hypothesized that the early intercalation contributes to the ventroflexion. This is because, in addition to the asymmetric actomyosin localization of the notochord, the asymmetric physiological factors of the tissues on the dorsal and ventral sides of the notochord could also be a factor in bending. To test this hypothesis, detailed observations of the ventral epidermis were made on *Admp* MO at the stage at which its epidermal cells complete cell-cell intercalation.

At st. 24, the WT *Ciona* tail epidermis finally forms eight distinct single-cell rows after cell-cell intercalation (Fig. 2CD) (Hotta et al., 2007; Pasini et al., 2006). The eight rows, consisting of three rows of dorsal, two rows of lateral, and three rows of dorsal epidermal cells, are aligned (Fig. 2D, WT). On the other hand, a 3D reconstructed image of the *Admp* MO embryo has shown a specific failure of the ventral three-rows' intercalation (Fig. 2D, *Admp* MO). Dorsomorphin treatment also shows a similar ventral midline intercalation defect in ventral epidermal cells (Suppl. Fig. 4). These results indicate that *Admp* regulates ventral epidermal cell-cell intercalation.

The ventral epidermal cells show the boat type morphology during ventroflexion

We suspected that abnormal cell intercalation of the ventral epidermis (Fig. 2D) in Admp/Bmp morphants was necessary to inhibit ventroflexion. To determine what morphological change has occurred in the ventral epidermal cells, we investigated the phenotype of WT embryos during the early intercalation at the single-cell level by reconstructed 3D imaging, especially focusing on the ventral midline epidermal cells. These 3D images of the intercalating cell revealed that these cells have a unique boat-type morphology (boat cell), a relatively larger area on the basal surface (Fig. 3AB, yellow areas) than the apical surface, having ridges at both ends in the left-right (LR) direction (Fig. 3AB, red areas). Boat cells with these characteristics can express tissue bending by compiling them alternately (Fig. 3C; Suppl. Fig. 5), like the actual ventral midline epidermal cells (Fig.3A). The boat cell has both a triangular-shaped section (Triangular-shaped section of Boat cell; TSBC) and a square-shaped section (Square-shaped section of Boat cell; SSBC), depending on the cutting plane (Fig. 3B). The median section image of the *Admp* MO tailbud embryo at st. 22 significantly decreased the number of TSBC (Fig. 3D and 3E; *Admp* MO, N= 12, WT, N = 7, p = 0.05×10^-5), indicating the decrease in the number of boat cells.

Admp/Bmp pathway translocates the pMLC to the apical side in epidermal cells

To know how this unique boat cell shape (Fig. 3A and 3B) was formed, we performed both phalloidin staining and the antibody staining of pMLC. The accumulation of both F-actin and pMLC was observed on the apical side of TSBC (Fig. 4A, WT arrowheads). On the other hand, the asymmetric localization of pMLC significantly decreased in *Admp* MO embryos (Fig. 4A, *Admp* MO and 3B; *Admp* MO, n = 7, WT, n = 9, p = 0.01). The pMLC localization was regulated by Admp/Bmp pathway, and bmp2/4 was ectopically expressed in epidermal cells (Fig. 4C). In ectopically Bmp-expressed embryos, the pSmad signal was detected in all

epidermal cells (Fig. 1E). Both pSmad signal and apical pMLC accumulation in WT embryos were not observed at the lateral side of epidermal cells (Fig. 4C, a frontal section of WT). On the other hand, in ectopically Bmp-expressed embryos, apical pMLC accumulation was observed on the lateral side of the epidermal cells (Fig. 4C, arrows of the frontal section in Dll-b>Bmp2/4). This result suggests that the pMLC translocates to the apical side depending on the pSmad signaling.

These results show that Admp controls the translocation of pMLC to the apical side of the ventral epidermal cells (Fig. 4D).

The cut of ventral epidermal cells causes relaxation of the ventroflexion

To verify whether the apical accumulation of pMLC in epidermal cells causes resistance to tail bending, the apical surface of the ventral or dorsal epidermal cells was cut using a laser cutter. The orientation of the cuts was along the apico-basal axis (Fig. 5, yellow lines).

As a result, the relaxation did not occur when the dorsal midline epidermal cells were cut, whereas the ventral midline epidermal cells showed relaxation to the dorsal side, indicating stress along with the AP axis at the ventral midline epidermal cells (Fig. 5A and 5B, Suppl. Mov. 2). We further investigated whether the ventral relaxation depends on the orientation of the cuts with AP axis vs. ML axis in ventral midline cells. As a result, the cut by AP orientation has no significant relaxation in the tail bending (data not shown). These results indicate that the boat cells apically accumulated pMLC caused AP stress in the ventral midline epidermis, enabling ventroflexion at st. 22.

The generation of boat cells and the relationship with cell-cell intercalation

Next, we investigated how the boat cells' shape changes and pMLC translocate during early intercalation, corresponding to the tail bending period (Fig. 6A). The

ventral view of the anti-pMLC stained embryo showed that ventral midline cells were undergoing cell-cell intercalation and eventually formed a row of median epidermal cells (ventral view in Suppl. Fig. 6).

The median cross-section indicated that the pMLC emerged at the anterior-posterior border of ventral midline epidermal cells from st. 21 (Fig. 6A, st. 21 arrowheads), translocated to the apical side, and made TSBCs at st. 22 (Fig. 6A, st. 22 arrowheads). At st. 23, the SSBCs – rather than the TSBCs – were observed at the midline plane (Fig. 6, st. 23; Suppl. Fig. 6), and finally, the apical accumulation of pMLC disappeared at st. 24 (Fig. 6, st. 24; Suppl. Fig. 6). From these observations, it is thought that the early intercalation without tissue elongation (Fig. 2B) until st. 22 is closely related to the intercalation of the boat cells (Fig. 6B).

As the cell-cell intercalation of the boat cell progresses, the cell shape of the median cross-section changes from TSBC to SSBC (Fig. 6A). However, this cell-cell intercalation processes up to st. 22 is the early intercalation period (Fig. 2B) and does not cause a change in AP length on the apical side (Fig. 6B, green arrows).

Therefore, this morphogenetic event resists notochord elongation force and lead tail bending (Fig. 6B, st. 20 to 22). On the other hand, in the later intercalation, the boat cells are enabled to relax the bending by the enlargement of the apical area, which finally causes AP elongation (Fig. 6B, yellow arrow st. 23).

Discussion

Admp is an upstream regulator of tail bending

Originally, the Admp/BMP pathway was identified as central in establishing, maintaining, and regenerating the DV axis among bilaterian animals (Gaviño and Reddien, 2011). In the ascidian, both gain- and loss-of-function experiments demonstrate that *Admp* expressed in the B-line medial vegetal cells acts as an endogenous inducer of the ventral epidermis midline (Pasini et al., 2006). *Admp* is

required for sensory neuron differentiation of the ventral epidermis via the *Tbx2/3* and *Msxb* genes (Waki et al., 2015). The phenotype of the *Msxb* MO (Suppl. Fig. 1C) indicates that tail bending was not regulated by *Msxb* but was regulated as a downstream pathway of *Admp*.

In this study, to identify the upstream regulator of tail bending in the *Ciona* tailbud embryos, we investigated the role of *Admp* and successfully found that *Admp* controls the ventroflexion (Fig. 1, Suppl.Mov. 1, Suppl. Fig. 1), the ventral epidermis cell-cell intercalation (Fig. 2), and the generation of the boat cells (Fig. 3) through the translocation of pMLC (Fig. 4) but does not control dorsiflexion (Fig.1A, yellow arrow). This is not to deny that genes other than Admp act on tissues other than the ventral epidermis to control flexion.

How does the intercalation of ventral midline cells contribute to tail bending? The ventral epidermis undergoing intercalation would have relatively slow elongation during st. 20 to st. 22 compared to the already intercalated dorsal epidermis (Fig. 2B). Considering the notochord as the main force of elongation (Dong et al., 2011; Hara et al., 2013; Lu et al., 2019), ventral epidermal cells might resist the AP elongation force of notochord during st. 20 to st. 22 and generate resistance temporally in the ventral midline epidermal cells. Supporting this, even if the dorsal midline epidermis elongates linearly, the ventral midline epidermis did not change the AP length at the beginning of the intercalation (Fig. 2B) and showed AP resistance (Fig. 5). The apically accumulated pMLC of the boat cells during intercalation (Fig. 4A) might contribute to the halt of the AP elongation of the apical side (Fig. 6, green arrows) of adjacent cells during tail bending. Actually, the bilateral-polarized shape of boat cells disrupted the polarity by Y27632 treatment (data not shown).

How does Admp/BMP signaling regulate both the cell-cell intercalation and the apico-basal polarity of the ventral epidermis via pMLC? In this study, it was indicated that the localization of the pMLC was observed not only at the AP cell-cell

border of intercalating cells (Suppl. Fig. 6) but also at the apical side (ventral side) translocated from the basal side (dorsal side) by pSmad signaling (Fig. 4C). Recent studies show that SMAD3 drives cell intercalation underlies secondary neural tube formation in the mouse embryo (Gonzalez-Gobartt et al., 2021). Moreover, it was known that the BMP-Rho-ROCK1 pathway targets MLC to control actin remodeling in fibroblasts (Konstantinidis et al., 2011). However, there have been no reports of Smad translocating MLC from the basal to the apical plane.

All midline epidermal cells intercalate and form apically constricted boat cells during early intercalation (Fig. 3). The relationship between midline intercalation and midline apical constriction is unclear, but both events are Admp-driven simultaneous behaviors of the ventral midline.

Model of ascidian ventroflexion

From our findings, *Admp* controls the ventroflexion of the tail during tailbud embryo stages, st. 18 to st. 22. The proposed model (Fig. 6C) is that Admp phosphorylates Smad in the ventral epidermis, pSmad controls the cell-cell intercalation in the ventral epidermis in which pMLC their translocate to make boat cell, generating resistance (Fig. 6, red arrows) in the ventral epidermis against notochord elongation force (Fig. 6, white arrow), and ultimately cause ventroflexion.

Actually, Y27632-treated embryos show cell shape elongation of ventral epidermal cells in the AP direction, supporting the possibility that pMLC exerts a resistance against notochord elongation in the AP direction (data not shown).

All midline epidermal cells undergoing early intercalation extend left and right and form boat-shaped cells. This process does not extend in the AP axial direction at the tissue level (Fig. 2B). We hypothesized that the myosin accumulation on the apical side of these boat-shaped cells resists the force of AP-axis notochord elongation in early intercalation and causes no ventral epidermis elongation (Fig. 6B). It has been reported that BMP regulates cell adhesion in early morphogenesis, such

as neural tube closure and gastrulation (von der Hardt et al., 2007; Smith et al., 2021). Cell adhesion molecules might also be involved in the generation of resistance.

A previous study indicated that the notochord generates asymmetric contraction force before st. 20 by the asymmetrical localization of actomyosin in the notochord (Lu et al., 2020). However, *Admp* MO embryos with straight tails still have ventral biases in notochord actomyosin (Suppl. Fig. 2). This indicated that *Admp* MO does not control asymmetrical localization of notochord actomyosin, and the localization seemed not enough to cause ventroflexion. The ventral accumulation of actomyosin in the notochord might reflect earlier morphogenetic events, such as the notochord intercalation, making a transient ventral groove (Munro and Odell, 2002).

Ventrofrextion promotes other tissue morphogenesis

What is the role of the ventroflexion? The cells and tissues of the developing embryos are changing their shape and arrangement from moment to moment, and we propose that those changes affect the mechanical state of other tissues where Admp was not originally involved. At this time, the newly appeared cells on the dorsal midline may irreversibly stabilize the whole-embryo shape, so the laser-cut experiment could not completely straighten the tail bending (Fig. 5A). Compared with Admp MO, the cell number of the ventral midline epidermis in WT at st. 22 did not change, but the cell number of the dorsal midline epidermis increased, even if Admp/Bmp signal was only exerted in the ventral epidermis (Suppl. Fig. 7). We propose that, in the WT embryo, ventroflexion has a mechanical effect on dorsal tissue, and because of promoting cell intercalation (Caussinus et al., 2008) and/or cell division (Campinho et al., 2013), the number of dorsal midline epidermal cells is increased (Suppl. Fig. 7).

The evolutionary roles of *Admp*

We conclude that *Admp* regulates ventroflexion during early to mid tailbud stages (st. 18 to st. 22) by the myosin-dependent force resistance in a small population of intercalating ventral midline epidermal cells against AP elongation force by the notochord. Our study provides insight into understanding the molecular and mechanical background that contributes to the conserved shape of the chordate embryo during the organogenesis period. Many of the published studies have not focused on the bending of the tailbud embryo; there seems to be many defects of tail bending in chordate embryos when many genes, as well as Admp/Bmp, are knocked down [zebrafish: (Esterberg et al., 2008; Willot et al., 2002); frog: (Dosch and Niehrs, 2000; Kumano et al., 2006)]. In invertebrate chordate animals, such as sea urchins and hemichordates, Admp is expressed at the ectoderm (Chang et al., 2016; Lowe et al., 2006) of embryos. It would be interesting to investigate whether the MLC regulation by Admp is conserved among primitive chordate embryogenesis and causes the body shape change in these animals. Since the apical surface is ventral to the cells of the ventral ectoderm in such small primitive chordates, the regulation of AP polarity at the cellular level by Admp/Bmp might directly influence the regulation of the DV polarity in the whole body.

To confirm whether the cell polarity-regulating function of *Admp* during embryo morphogenesis that we detect in this study is evolutionarily conserved among animals, the morphogenetic roles of *Admp* in other animals should be investigated in future work.

Materials and methods

Ascidian samples

C. robusta (*C. intestinalis* type A) adults were obtained from Maizuru Fisheries Research Station (Kyoto University, Kyoto, Japan), Onagawa Field Center (Tohoku University, Sendai, Japan), and Misaki Marine Biological Station (University of Tokyo, Tokyo, Japan) through the National Bio-Resource Project (NBRP, Japan) and

from the Roscof Marine Station (Roscof, France). Eggs were collected by dissection of the gonoducts. After artificial insemination, fertilized eggs were incubated at 20°C until fixation or observation. Developmental stages followed Hotta's stages (Hotta et al., 2007; Hotta et al., 2020). In inhibiting phosphorylation of 1P myosin, Y27632 (nacalai tesque, Japan) was applied to embryos at 10 μM after 7 hpf (late neurula, st. 16). Dorsomorphin (Sigma-Aldrich) was applied to embryos at 10 μM after fertilization.

Immunostaining and quantifying pMLC intensity

To detect activation of the Admp/BMP signaling pathway, we followed the same method described previously (Waki et al., 2015). The signal was visualized with a TSA kit (Invitrogen) using horseradish peroxidase-conjugated goat anti-rabbit immunoglobulin-G and Alexa Fluor 488 tyramide.

The method of pMLC antibody staining was as follows. Embryos were fixed in 3.7% formaldehyde in seawater for 30 min and then rinsed with phosphate-buffered saline with Tween (PBST; 0.2% Triton-X in PBS) for 3 h. Embryos were incubated in PBST containing 10% goat serum for 3 h at room temperature or overnight at 4°C. The primary antibody (anti-rabbit Ser19 phosphorylated-1P-myosin, Cell Signaling, USA) was diluted at 1:50 and then incubated for 3 h at room temperature or overnight at 4°C. The primary antibody was washed with PBST for 3 h. A poly-horseradish peroxidase (HRP) secondary antibody (goat anti-rabbit IgG, Alexa Fluor 488 Tyramide SuperBoost Kit, USA) was applied for 3 h and washed in PBST for 3 h. Alexa Fluor dye tyramide (Alexa Fluor 488 Tyramide SuperBoost Kit) was added to the reaction buffer for 5 to 8 min to induce a chemical HRP reaction. Embryos were dehydrated through an isopropanol series and finally cleared using a 2:1 mixture of benzyl benzoate and benzyl alcohol.

pMLC accumulation was quantified by measuring the intensity along the ventral tail epidermis using Fiji image analysis software. The signal in the brain

region was taken as the positive control because its signal was detected even in Y27632 treated embryos, indicating RhoA kinase (ROCK)-independent expression. The relative intensity of pMLC normalized to the intensity of the brain region in each individual was calculated by ImageJ for the comparative analysis among different individuals.

Laser-cutter experiment

UV-laser cutting experiments were performed on tailbud *Ciona* embryos. An inverted Axio Observer Z1 (Zeiss) microscope equipped with a confocal spinning disk (Andor Revolution Imaging System, Yokogawa CSU-X1), a Q-switched solid-state 355 nm UV-A laser (Powerchip, Teem Photonics), a C-APOCHROMAT 63x/1.2 W Korr UV-VIS-IR water immersion objective (Behrndt et al., 2012), and a home-made cooling stage was used. The membrane of tail epidermal cells of tailbud embryos was labeled with FM-64 (ThermoFisher). Each ventral midline epidermal cell was cut along the apico-basal axis (5 to 10 µm lines each) by applying 25 UV pulses at 0.7 kHz. The embryos were imaged every 0.2 s frame rate with an exposure time of 150 ms. Single fluorescent images were used to measure tail relaxation 3 s post-ablation, and the percentage of relaxation was calculated as the area of movement of the tail region 3 s after laser cutting.

Gene knock-down and overexpression

The MOs (Gene Tools, LLC) against *Msxb* and *Admp*, which block translation, were designed according to the previous study (Imai et al., 2006; Waki et al., 2015); *Admp*, 5′-TATCGTGTAGT TTGCTTTCTATATA-3′; *Msxb*, 5′-ATTCGTTTACTGTCATTTTTAATTT-3′. These MOs at 0.25 to 0.50 mM were injected into an unfertilized egg and incubated until observation. To know the phenotype of *Admp* MO embryo at the single-cell level, embryos were stained by Alexa 546 phalloidin (Thermo Fisher).

The DNA constructs used for overexpression of Bmp2/4 under the Dlx.b upstream sequence (Ciinte.REG.KH.C7.630497–632996|Dlx.b) were used previously (Imai et al., 2012). These DNA constructs were introduced by electroporation.

Acknowledgments

Ciona intestinalis adults were provided by Dr. Yutaka Satou (Kyoto University) and Dr. Manabu Yoshida (the University of Tokyo) with support from the National Bio-Resource Project of AMED, Japan. We thank Dr. Hidehiko Hashimoto and Mr. Yuji Mizotani for technical information with 1P-myosin antibody staining.

We thank Dr. Yutaka Sato for the valuable discussion of *Admp* and for sharing unpublished RNA-seq data, the DNA construct of Bmp2/4 under the Dlx.b upstream sequence. We thank Ms. Maki Kogure for constructing the 3DCAD of the intercalating epidermal cell.

Competing interests

The authors declare no competing or financial interests.

Author contributions

Y.S.K., H.M., W.C.K, and K.H. designed and performed research. Y.S.K., W.C.K, R.G., and H.M. analyzed data. W.C.K., B.G., and K.H. performed the laser cutter experiments. H.M. performed a 1P-myosin analysis. Y.S.K. and K.H. wrote the manuscript. K.O. and C.P.H critically revised the manuscript. K.H. and K.O. supervised the research.

Funding

This work was supported by JSPS KAKENHI, Grant Numbers JP16H01451, JP16K07426 and 21H00440.

Data availability

All data generated or analyzed during this study are included in the manuscript and supporting files.

Figure legends

Fig. 1 *Admp* affects the tail bending of early tailbud stage embryo, and pSmad was detected at ventral midline epidermis.

(A) Time-lapse movie of WT and *Admp* MO embryos (N=6/6). WT and *Admp* MO embryos were developed in the same dish, and WT embryos were stained by NileBlue B to distinguish them. Note that *Admp* MO suppressed ventral tail bending ("ventroflexion") during early to mid taibud stages (red double-headed arrow) but not dorsal tail bending ("dorsiflexion") during the late tailbud stage (yellow double-headed arrow) after "relaxation" (blue double-headed arrow) at the beginning of late tailbud stage. The developmental stage and time after fertilization are shown in each WT picture. Scale bar = 100 μm. A: anterior, P: posterior, D: dorsal, and V: ventral. (B) The definition of the bending angle. The bending angle of the embryo tail was defined as the intersection angle of the straight line perpendicular to the neural tube of the trunk and the anterior-posterior border of the notochord cell, which is the 20th from the anterior side. (C) Quantification of the bending angle θ of WT (n=8) and *Admp* MO (n=5~15) embryo at st. 18, st. 20, and st. 22. The bending angle was significantly reduced in *Admp* MO embryos. (D) Quantification of the bending angle θ of WT (n=8), DMSO-treated embryos (n=6~7), and Dorsomorphin-treated embryos (n=9~12). The bending angle was significantly reduced in Dorsomorphin-treated embryos.

(E) An antibody staining against phosphorylated Smad1/5/8 (green). The Admp/Bmp signals were detected from the late gastrula at ventral midline cells in WT (parenthesis). On the other hand, no signals were detected in *Admp*-MO. Ectopic signals were detected at the whole-epidermal cells in the Dll-b>Bmp2/4 embryo (right bottom panel). Scale bar = 50 μm.

Fig. 2 Comparison of the phenotype of *Admp* MO with WT embryo.

(A) The measurement of the tail length of the dorsal side (red line) and the ventral side (blue line). (B) Time course of dorsal outline length (red line) and the tail region's ventral outline length (blue line). Dorsal A-P length of the tail epidermis (red) increases earlier than that of ventral A-P (blue). The ventral A-P length does not change during early intercalation (red double-headed arrow). So, the gap between them is increasing in this period. The ventral A-P length increased at late intercalation (double-headed arrow), and the gap decreased. Each dotted line indicates the corresponding developmental *Ciona* stage. At stage 24, both the dorsal A-P and the ventral A-P have the same length.

(C) The schematic alignment of the tail epidermal cells of WT embryo at st. 24. The cell-cell intercalation of the tail epidermis has finished at st. 24. The tail epidermal cells consist of eight rows: dorsal (yellow), two dorsal medio-lateral (green), ventral (red), two ventral medio-lateral (orange), and two lateral (blue) rows.

(D) The alignment of the tail epidermal cells of WT and *Admp* MO embryo at st. 24. There is a specific inhibition of the intercalation of the ventral rows (red and orange) in the *Admp* MO embryo (N = 4 in WT and 4 in *Admp* MO).

Fig. 3 Three-dimensional reconstruction of ventral midline epidermal cells during tail bending.

(A) The 3D model that reflects the shape of each midline ventral epidermal cell at st. 22 was reconstructed using Avizo6 software (inside of red rectangular). Representative morphology of ventral midline cells is shown (inside the green rectangle). Each cell is bipolar laterally and has protrusions from basal parts. Note that the apical area (red) is smaller than the basal area (yellow).

(B) The 3D model reflects the shape of ventral epidermal cells in (A). The ventral epidermal cells show a unique shape, a “boat cell”. The sections of the boat cell show triangular-shaped (TSBC) or square-shaped (SSBC) depending on the plane.

(C) Schematic drawing of the cell-cell intercalation of the ventral midline epidermal cells using boat cells during the tail bending period. The ventral midline epidermis consists of boat cells with a smaller apical domain area than the basal domain; the overall tissue becomes bending (blue arrow). The orange cell’s midline section (cut in the red dotted plane) shows TSBC. The orange cell starts intrusion from basolateral sides with pMLC protrusions (red-colored). The 3D models were generated by FUSION 360 educational ver. (Autodesk).

(D) Midline section view of WT tailbud embryo and *Admp* MO embryo at st. 22 by staining of F-actin. Arrowheads indicate the position of TSBC. The regions in a yellow rectangle are enlarged, showing a TSBC. The regions in a green rectangle are enlarged, showing an SSBC.

(E) The ratio of the number of TSBC and the number of midline cells. It has been reported the driving forces of the tail bending originate in the anterior part of the tail (Lu et al., 2020). Therefore, we counted the number of TSBC in the anterior part of the tail. TSBCs were significantly reduced in *Admp* MO embryos. Asterisk indicates statistically significant (t-test, *: $p < 0.05$). The error bar indicates S.D. (WT, N = 8; Admp MO, N = 6).

Fig. 4 The distribution of pMLC of tail epidermis depends on the Admp/bmp pathway.

(A) Double staining of F-actin and phosphorylated myosin light chain (pMLC) of the ventral midline of WT and *Admp* MO embryo at st. 22. Both F-actin and pMLC accumulated at the apical side of triangular cells (arrowheads). The loci of the

measurement of the relative pMLC intensity ratio between the apical and basal side of the epidermis in WT and *Admp* MO(B) were shown in yellow lines.

(B) Relative pMLC intensity ratio between the apical and basal side of the epidermis in WT (N = 10) and *Admp* MO (N = 7). Asterisk indicates statistically significant (t-test, *: $p<0.05$, **: $p<0.01$). The error bar indicates S.D.

(C) The distribution of pMLC in WT and *Dll-b>Bmp2/4* at st. 22. In the midline section, the pMLC was distributed at the apical TSBCs of the ventral midline epidermis in both WT and Dll-b>Bmp2/4 (arrows in red rectangles). On the other hand, in the frontal section, the apical TSBCs of the lateral epidermis was observed in Dll-b>Bmp2/4 embryo (arrows in orange rectangle), but there was no signal of pMLC in the lateral epidermis in WT. The white dotted lines indicate the section plane of the frontal sections.

(D) The schematic of the difference in the distribution of pMLC (red) among WT, *Admp* MO and *Dll-b>Bmp2/4* embryos. The orange-colored cell sections are TSBC.

Fig. 5. Laser-cut experiment for the AP cell-cell border of the tail epidermis.

(A) Laser-cutting of the wild type's dorsal and ventral midline epidermis at st. 22. Epidermal cells are a monolayer. We cut each cell in an apico-basal direction (yellow lines). (B) The movement of the area before and after the laser cut was calculated as relaxation (N = 5). Asterisk indicates statistically significant (t-test, *: $p< 0.05$). The error bar indicates S.D.

Fig. 6. Relationship between the change of the distribution of pMLC and the tail bending during intercalation of midline epidermal cells.

(A) (top) The antibody staining of 1-phosphorylated-myosin (pMLC) from st. 20 to 24 in WT. Scale bar = 50 μm. (middle) The enlarged view of the dotted rectangle in each stage. Arrowheads show pMLC accumulation in the apical domain of the ventral midline epidermal cells. (bottom) The schematic drawing of the distribution of pMLC (shown in red). In st. 20, pMLC localized the basal side of the epidermis. In st. 21, pMLC has appeared at the AP cell border of ventral midline epidermal cells. At st. 22, the pMLC accumulated at the apex of the apical domain and the cell shape changed into TSBC of the boat cell in Figure 3C (orange-colored cell). The pMLC localization at the basal side was reduced. At st. 23, the apex of the apical domain becomes broader. At st. 24, the pMLC asymmetrical distribution disappears.

(B) The schematic model explains the halt of the AP elongation during the early intercalation period. At the beginning of the intercalation, the total AP length of the midline cells was shown as a green arrow (st. 20). During early intercalation, the ventral epidermal cells change cell shape to become boat cells, and the boat cells start to intrude each other from the basal plane, but the total AP length of the apical side was not changed (green arrow) because apically accumulated pMLC (st. 22) resists the AP elongation force of notochord. In late intercalation, the boat cell intercalates the basal side and the apical side and the apical area increases, allowing the elongation of AP length (yellow arrow) of the apical side (st. 23).

(C) Model of embryonic tail bending in *Ciona*. Admp/BMP signaling (green dots) transmits the signal to the ventral midline epidermal cells as phosphorylated Smad from neurula to the initial tailbud. pSmad translocates the localization of the pMLC from the basal side (dorsal side) to the apical side (ventral side), which changes the cell polarity and promotes the cell-cell intercalation of the ventral midline epidermal cells during early to mid-tailbud stages (st. 20 to st. 23). The ongoing mediolateral intercalation at the ventral epidermis confers a resistance (red arrowheads) to AP elongation force (white arrow) that is possibly provided by the notochord, which causes the bending tail shape in the *Ciona* tailbud embryo at st. 22. On the other hand,

the *Admp* MO or dorsomorphin treatment disrupts the cell polarity and causes the no tail-bending embryo at st. 20–23 and incomplete intercalation at st. 24 (the flow by the green rectangle). The final overall embryo shape at st. 24 is similar among WT and *Admp* MO embryos, but the ventral cell-cell intercalation was disrupted (red and orange gradation-colored cells). Thus, Admp/BMP signaling, apart from its known role in peripheral nervous system (PNS) differentiation, regulates temporal tail bending during early to middle tailbud stages (st. 20 to st. 23).

Suppl. Mov. 1. Time-lapse movie of WT (left) and *Admp* MO (right) embryo from late neurula stage 16 to late tailbud stage 25.

Both embryos are incubated in the same dish. The WT embryo was stained with NileBlue B (Matsumura et al., 2020). The movie frame was surrounded by different colors depending on the tail morphology. red: ventroflexion, blue: relaxation of ventroflexion, yellow: dorsiflexion.

Suppl. Mov. 2. Laser cutting experiment of the midline tail epidermis.

The dorsal (left) and ventral (right) midline epidermal AP cell borders of the WT mid-tailed embryos were cut with a laser cutter. The arrowheads indicate the cutting point by the laser cutter. The angle of the ventroflexion was relaxed when cut on the ventral side but not on the dorsal side, indicating the AP stress of the ventral midline epidermis (N = 3 each).

Suppl. Fig. 1. Morphants of tail bending.

(A) Mid-tailbud stage embryo of WT, DMSO treatment, and dorsomorphin. DMSO and dorsomorphin were treated after the mid neurula stage (st. 15). The dorsomorphin-treated embryo did not bend its tail, similar to the *Admp* MO embryo (Fig.1A).

(B) Midline section view of WT, dorsomorphine-treated and *Admp* MO embryo at st. 18, st. 20, and st. 22 by F-actin staining. The dorsomorphin-treated embryo did not bend its tail (N = 10/10, 12/12 and 9/9), similar to the *Admp* MO embryo (N = 5/5, 13/13 and 15/15).

(C) The phenotype of *Msx-b* MO embryo at st. 22 in one experiment. The ventral tail bending was normally observed. Note that similar phenotypes were reported (Waki et al., 2015).

Abbreviations: A, anterior; D, dorsal; V, ventral; P, posterior

Suppl. Fig. 2. The asymmetrical actomyosin localization of the notochord.

(A) F-actin localization of notochord in both WT and *Admp* MO was measured on the yellow lines across the dorso-ventral (DV) axis. Abbreviations: A, anterior; D, dorsal; V, ventral; P, posterior.

(B) The intensity ratio between ventral and dorsal F-actin. The ratio is calculated from the peak intensity values in (A) data. If the intensity of the ventral side (red arrow in A) is stronger than the dorsal side (orange arrow in A), the ratio becomes more than 1. In Admp MO embryos, F-actin is significantly localized ventrally (WT, N=8; Admp MO, N=10). Asterisks indicate statistical significance (t-test, *: $p < 0.05$). The error bar indicates S.D.

Suppl. Fig. 3 The alignment of the tail midline epidermal cells during the tailbud period.

From 3D reconstructed confocal stack images by F-actin staining of tailbud embryos (st. 18 in A, st. 19 in B, st. 20 in C, st. 21 in D, st. 22 in E, st. 23 in F and st. 24 in G), cell shapes of both dorsal and ventral midline epidermal cells are traced (yellow lines). Note that cell-cell intercalation completes earlier on the dorsal midline than on the ventral midline.

Suppl. Fig. 4 The alignment of the tail epidermal cells of DMSO-treated and Dorsomorphin-treated embryo at st. 24.

The cell-cell intercalation was completed in the DMSO-treated embryo (left), and the tail epidermal cells consist of eight rows: dorsal (yellow), two dorsal medio-lateral (green), ventral (red), two ventral medio-lateral (orange), and two laterals (blue)

rows. On the other hand, there is a ventral-side specific inhibition of the intercalation (red and orange gradation-colored cells) in dorsomorphin-treated embryo (right). (N = 2 in DMSO and 2 in dorsomorphin)

Suppl. Fig. 5 Boat cells make up the bending of the tissue.

(A) Development view of a 3D model schematically showing the boat cell in the ventral midline epidermis (see Fig. 3A–C).

(B) A combination of boat cells representing the ventral midline epidermis during intercalation. (C) Lateral view of (B). The tissue is bending, as shown in the blue arrow.

Suppl. Fig. 6. pMLC antibody staining during tailbud period.

(Aa–Hc') Antibody staining of pMLC from st. 18 to st. 24 in wild type (rows A to G) and st. 22 in Y27632-treated (row H) embryos. Arrowheads show pMLC accumulation in the ventral midline epidermal cells. The part surrounded by the dotted square is enlarged to the panel on the right. Brackets indicate the range of the midline epidermal region. The midline epidermal cells are intercalated, narrowing the region (see Suppl. Fig. 2). Scale bar = 20 μm.

Suppl. Fig. 7 Comparison of the number of midline epidermal cells between the dorsal and ventral sides.

The number of ventral midline epidermal cells is counted. (A) The number of ventral midline cells in WT and Admp MO embryo. (B) The number of dorsal midline cells in WT and Admp MO embryo. Asterisk indicates statistically significant (t-test, ***: $p<0.001$). The error bar indicates S.D. (WT, N = 8; Admp MO, N = 9~11)

References

Blitz, I. L. and Cho, K. W. Y. (2009). Finding partners: How BMPs select their targets. *Dev. Dyn.* **238**, 1321–1331.

Campinho, P., Behrndt, M., Ranft, J., Risler, T., Minc, N. and Heisenberg, C.-P. (2013). Tension-oriented cell divisions limit anisotropic tissue tension in epithelial spreading during zebrafish epiboly. *Nat. Cell Biol.* **15**, 1405–1414.

Caussinus, E., Colombelli, J. and Affolter, M. (2008). Tip-Cell Migration Controls Stalk-Cell Intercalation during Drosophila Tracheal Tube Elongation. *Curr. Biol.* **18**, 1727–1734.

Chang, Y.-C., Pai, C.-Y., Chen, Y.-C., Ting, H.-C., Martinez, P., Telford, M. J., Yu, J.-K. and Su, Y.-H. (2016). Regulatory circuit rewiring and functional divergence of the duplicate admp genes in dorsoventral axial patterning. *Dev. Biol.* **410**, 108–18.

De Robertis, E. M. M. (2009). Spemann's organizer and the self-regulation of embryonic fields. *Mech. Dev.* **126**, 925–941.

Dong, B., Deng, W. and Jiang, D. (2011). Distinct cytoskeleton populations and extensive crosstalk control Ciona notochord tubulogenesis. *Development* **138**, 1631–1641.

Dosch, R. and Niehrs, C. (2000). Requirement for anti-dorsalizing morphogenetic protein in organizer patterning. *Mech. Dev.* **90**, 195–203.

Esterberg, R., Delalande, J.-M. and Fritz, A. (2008). Tailbud-derived Bmp4 drives proliferation and inhibits maturation of zebrafish chordamesoderm. *Development* **135**, 3891–3901.

Gaviño, M. A. and Reddien, P. W. (2011). A Bmp/Admp Regulatory Circuit Controls Maintenance and Regeneration of Dorsal-Ventral Polarity in Planarians. *Curr. Biol.* **21**, 294–299.

Gonzalez-Gobartt, E., Blanco-Ameijeiras, J., Usieto, S., Allio, G., Benazeraf, B. and Martí, E. (2021). Cell intercalation driven by SMAD3 underlies secondary neural tube formation. *Dev. Cell* **56**, 1147-1163.e6.

Hara, Y., Nagayama, K., Yamamoto, T. S., Matsumoto, T., Suzuki, M. and Ueno, N. (2013). Directional migration of leading-edge mesoderm generates physical forces: Implication in Xenopus notochord formation during gastrulation. *Dev. Biol.* **382**, 482–495.

Hotta, K., Yamada, S., Ueno, N., Satoh, N. and Takahashi, H. (2007). Brachyury-downstream notochord genes and convergent extension in Ciona intestinalis embryos. *Dev. Growth {\&} Differ.* **49**, 373–382.

Hotta, K., Dauga, D. and Manni, L. (2020). The ontology of the anatomy and development of the solitary ascidian Ciona: the swimming larva and its metamorphosis. *Sci. Rep.* **10**, 1–16.

Imai, K. S., Levine, M., Satoh, N. and Satou, Y. (2006). Regulatory Blueprint for a Chordate Embryo. *Science (80-.).* **312**, 1183–1187.

Imai, K. S., Daido, Y., Kusakabe, T. G. and Satou, Y. (2012). Cis-acting transcriptional repression establishes a sharp boundary in chordate embryos. *Science (80-.).* **337**, 964–967.

Klaus., S. (1983). *The evolution of patterning mechanisms: gleanings from insect embryogenesis and spermatogenesis.* (ed. GoodwinBC, HolderN, W.) Cambridge University Press.

Konstantinidis, G., Moustakas, A. and Stournaras, C. (2011). Regulation of myosin light chain function by BMP signaling controls actin cytoskeleton remodeling. *Cell. Physiol. Biochem.* **28**, 1031–1044.

Kumano, G., Ezal, C. and Smith, W. C. (2006). ADMP2 is essential for primitive blood and heart development in Xenopus. *Dev. Biol.* **299**, 411–423.

Lowe, C. J., Terasaki, M., Wu, M., Freeman, R. M., Runft, L., Kwan, K., Haigo, S., Aronowicz, J., Lander, E., Gruber, C., et al. (2006). Dorsoventral Patterning in Hemichordates: Insights into Early Chordate Evolution. *PLoS Biol.* **4**, e291.

Lu, Q., Bhattachan, P. and Dong, B. (2019). Ascidian notochord elongation. *Dev. Biol.* **448**, 147–153.

Lu, Q., Gao, Y., Fu, Y., Peng, H., Shi, W., Li, B., Lv, Z., Feng, X.-Q. and Dong, B. (2020). Ciona embryonic tail bending is driven by asymmetrical notochord contractility and coordinated by epithelial proliferation. *Development* **147**,.

Matsumura, K. D., Nakamura, M. J., Koizumi, W. C., Hotta, K. and Oka, K. (2020). Different strategies for tissue scaling in dwarf tailbud embryos revealed by single-cell analysis. *Dev. Biol.* **460**, 215–223.

Miyamoto, D. M. and Crowther, R. J. (1985). Formation of the notochord in living ascidian embryos. *J. Embryol. Exp. Morphol.* **86**, 1–17.

Munro, E. M. and Odell, G. (2002). Morphogenetic pattern formation during ascidian notochord formation is regulative and highly robust. *Development* **129**, 1–12.

Pasini, A., Amiel, A., Rothbächer, U., Roure, A., Lemaire, P. and Darras, S. (2006). Formation of the Ascidian Epidermal Sensory Neurons: Insights into the Origin of the Chordate Peripheral Nervous System. *PLoS Biol.* **4**, e225.

Richardson, M. K., Hanken, J., Gooneratne, M. L., Pieau, C., Raynaud, A., Selwood, L. and Wright, G. M. (1997). There is no highly conserved embryonic stage in the vertebrates: implications for current theories of evolution and development. *Anat. Embryol. (Berl).* **196**, 91–106.

Roure, A. and Darras, S. (2016). Msxb is a core component of the genetic circuitry specifying the dorsal and ventral neurogenic midlines in the ascidian embryo. *Dev. Biol.* **409**, 277–287.

Sehring, I. M., Dong, B., Denker, E., Bhattachan, P., Deng, W., Mathiesen, B. T. and Jiang, D. (2014). An Equatorial Contractile Mechanism Drives Cell Elongation but not Cell Division. *PLoS Biol.* **12**, e1001781.

Smith, H. M., Khairallah, S. M., Nguyen, A. H., Newman-Smith, E. and Smith, W. C. (2021). Misregulation of cell adhesion molecules in the Ciona neural tube closure mutant bugeye. *Dev. Biol.* **480**, 14–24.

Spemann, H. (1987). Embryonic Induction. *Am. Zool.* **27**, 575–579.

Ubisch, V. L. v. (1939). KEIMBLATTCHIMÄRENFORSCHUNG AN SEEIGELLARVEN. *Biol. Rev.* **14**, 88–103.

von der Hardt, S., Bakkers, J., Inbal, A., Carvalho, L., Solnica-Krezel, L., Heisenberg, C.-P. and Hammerschmidt, M. (2007). The Bmp Gradient of the Zebrafish Gastrula Guides Migrating Lateral Cells by Regulating Cell-Cell Adhesion. *Curr. Biol.* **17**, 475–487.

Waki, K., Imai, K. S. and Satou, Y. (2015). Genetic pathways for differentiation of the peripheral nervous system in ascidians. *Nat. Commun.* **6**, 8719.

Willot, V., Mathieu, J., Lu, Y., Schmid, B., Sidi, S., Yan, Y. L., Postlethwait, J. H. H., Mullins, M., Rosa, F., Peyriéras, N., et al. (2002). Cooperative action of ADMP- and BMP-mediated pathways in regulating cell fates in the zebrafish gastrula. *Dev. Biol.* **241**, 59–78.

Zhou, J., Pal, S., Maiti, S. and Davidson, L. A. (2015). Force production and mechanical accommodation during convergent extension. *Development* **142**, 692–701.

A

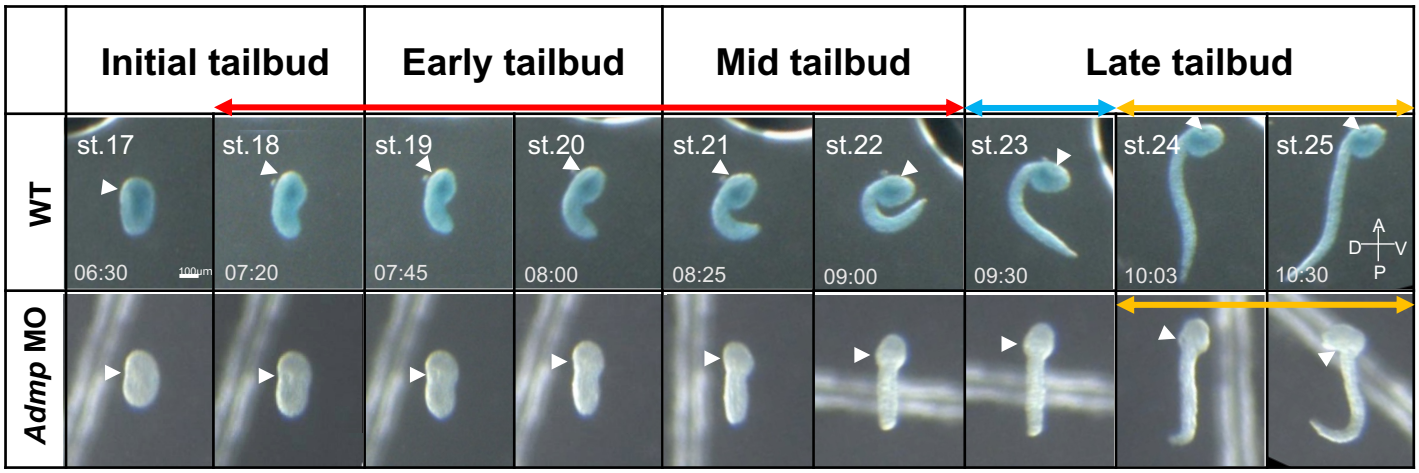

B

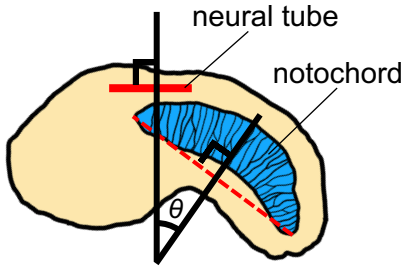

Definition of bending angle

C

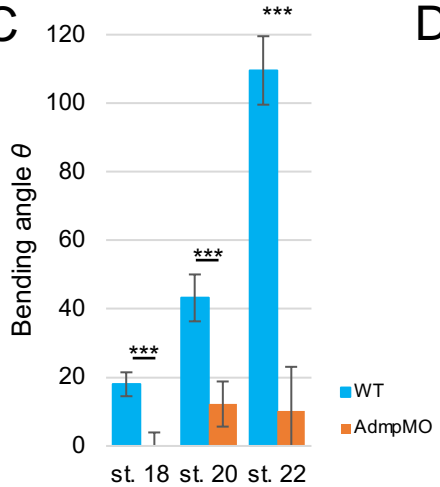

D

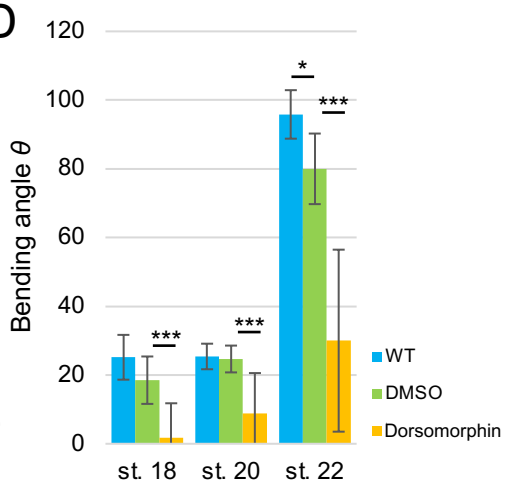

E

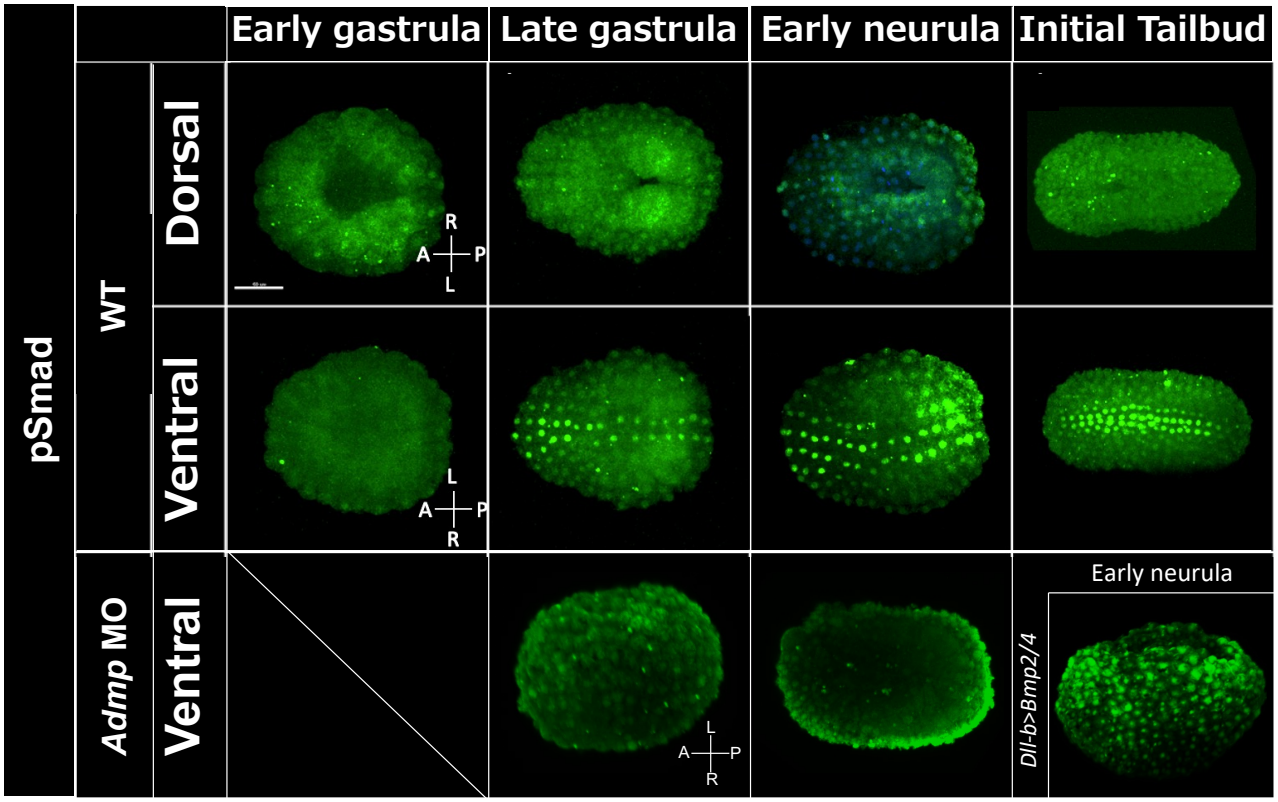

Fig. 1

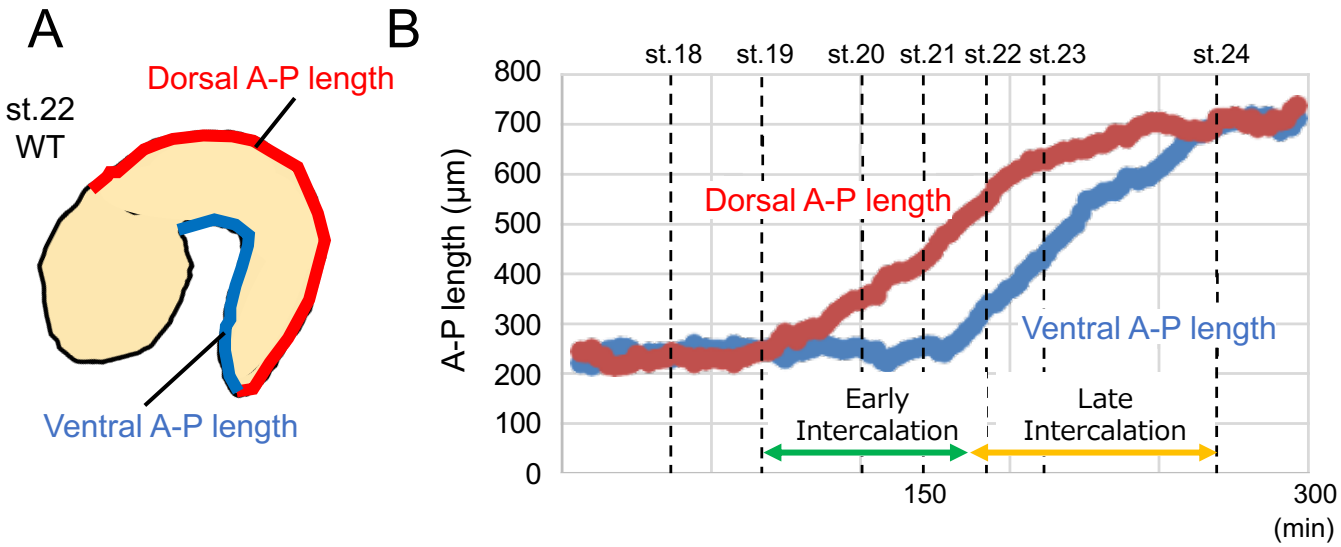
A
st.22
WT
Dorsal A-P length
Ventral A-P length
B
st.18
st.19
st.20
st.21
st.22
st.23
st.24
A-P length (μm)
800
700
600
500
400
300
200
100
0
Dorsal A-P length
Ventral A-P length
Early
Intercalation
Late
Intercalation
150
300
(min)

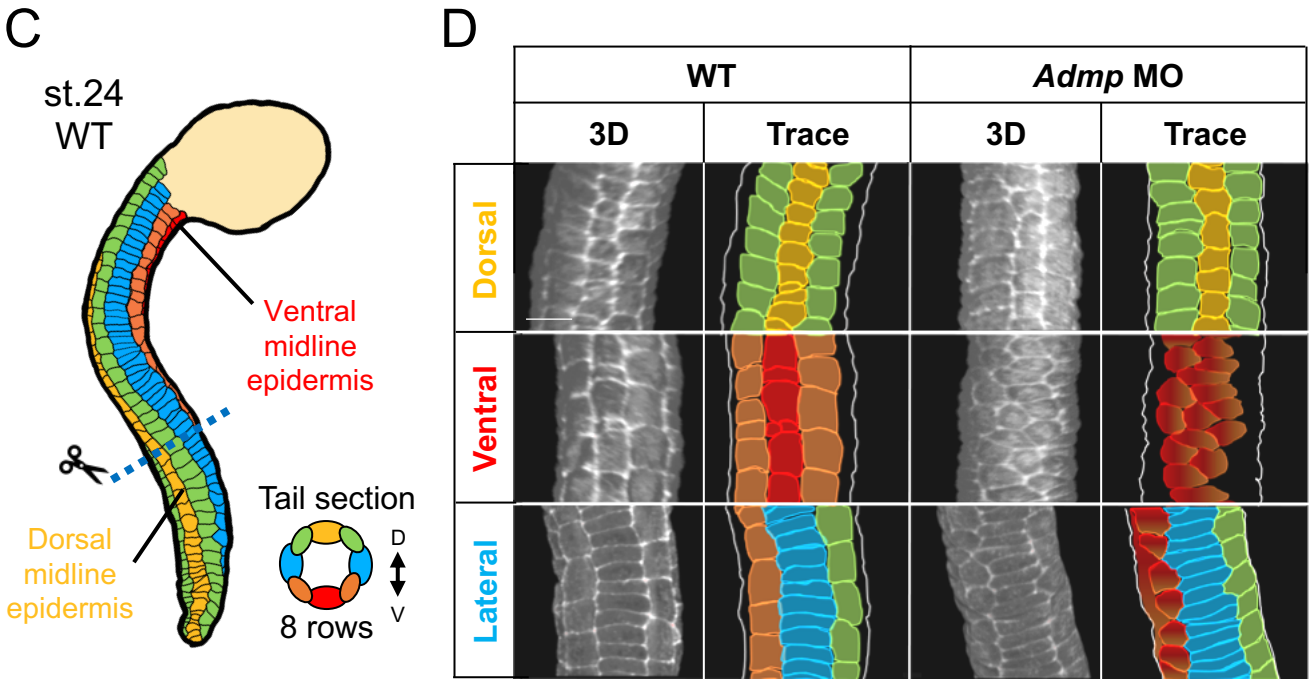
C
st.24
WT
Ventral
midline
epidermis
Dorsal
midline
epidermis
Tail section
D
V
8 rows
D
WT
Admp MO
3D
Trace
3D
Trace
Dorsal
Ventral
Lateral

Fig. 2

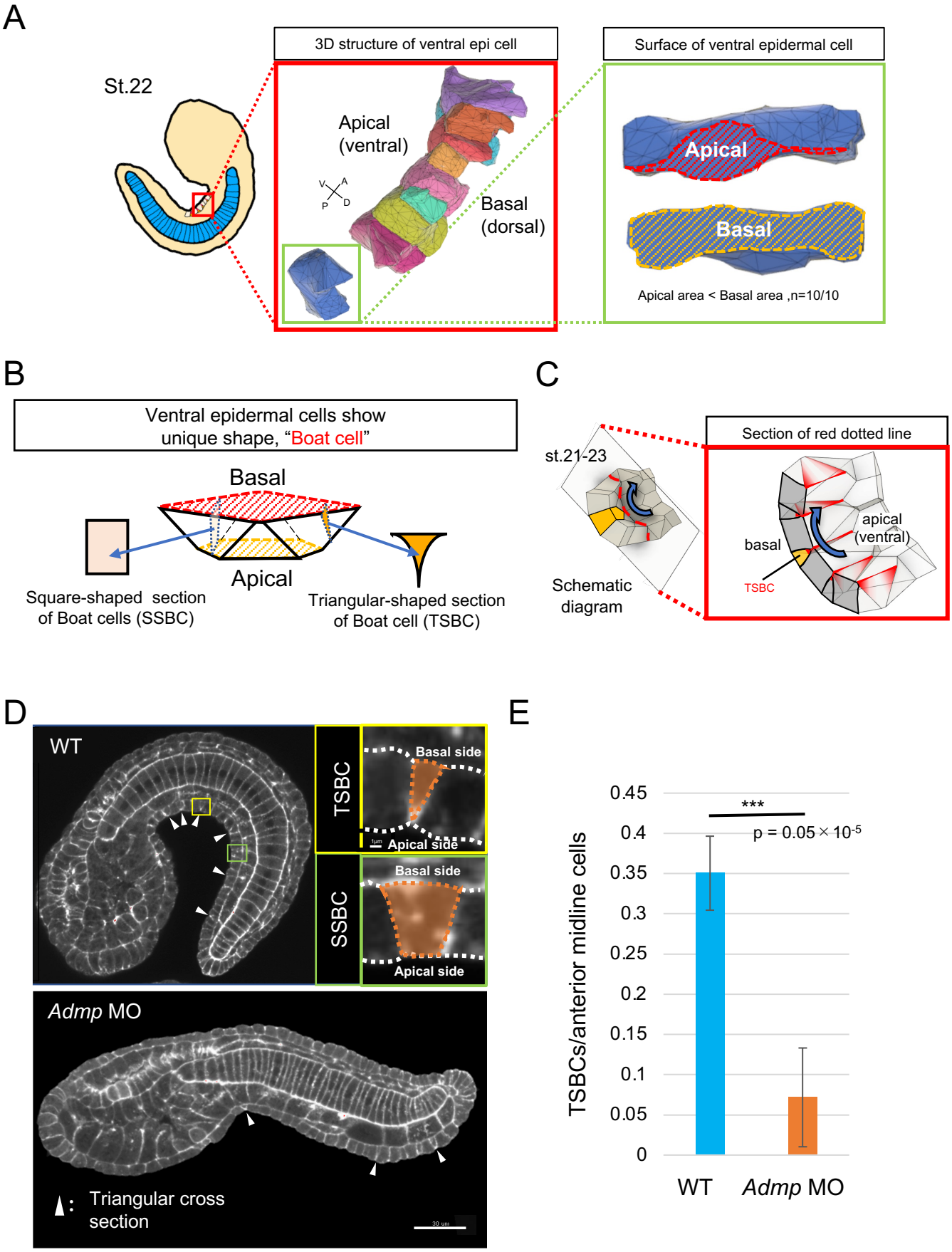
A
St.22
3D structure of ventral epi cell
Apical
(ventral)
Basal
(dorsal)
V
A
P
D
Surface of ventral epidermal cell
Apical
Basal
Apical area < Basal area ,n=10/10
B
Ventral epidermal cells show
unique shape, "Boat cell"
Basal
Apical
Square-shaped section
of Boat cells (SSBC)
Triangular-shaped section
of Boat cell (TSBC)
C
st.21-23
Schematic
diagram
Section of red dotted line
basal
apical
(ventral)
TSBC
D
WT
TSBC
Basal side
Apical side
SSBC
Basal side
Apical side
Admp MO
Triangular cross
section
E
TSBCs/anterior midline cells
0.45
0.4
0.35
0.3
0.25
0.2
0.15
0.1
0.05
0
***
p = 0.05 × 10-5
WT
Admp MO

Fig. 3

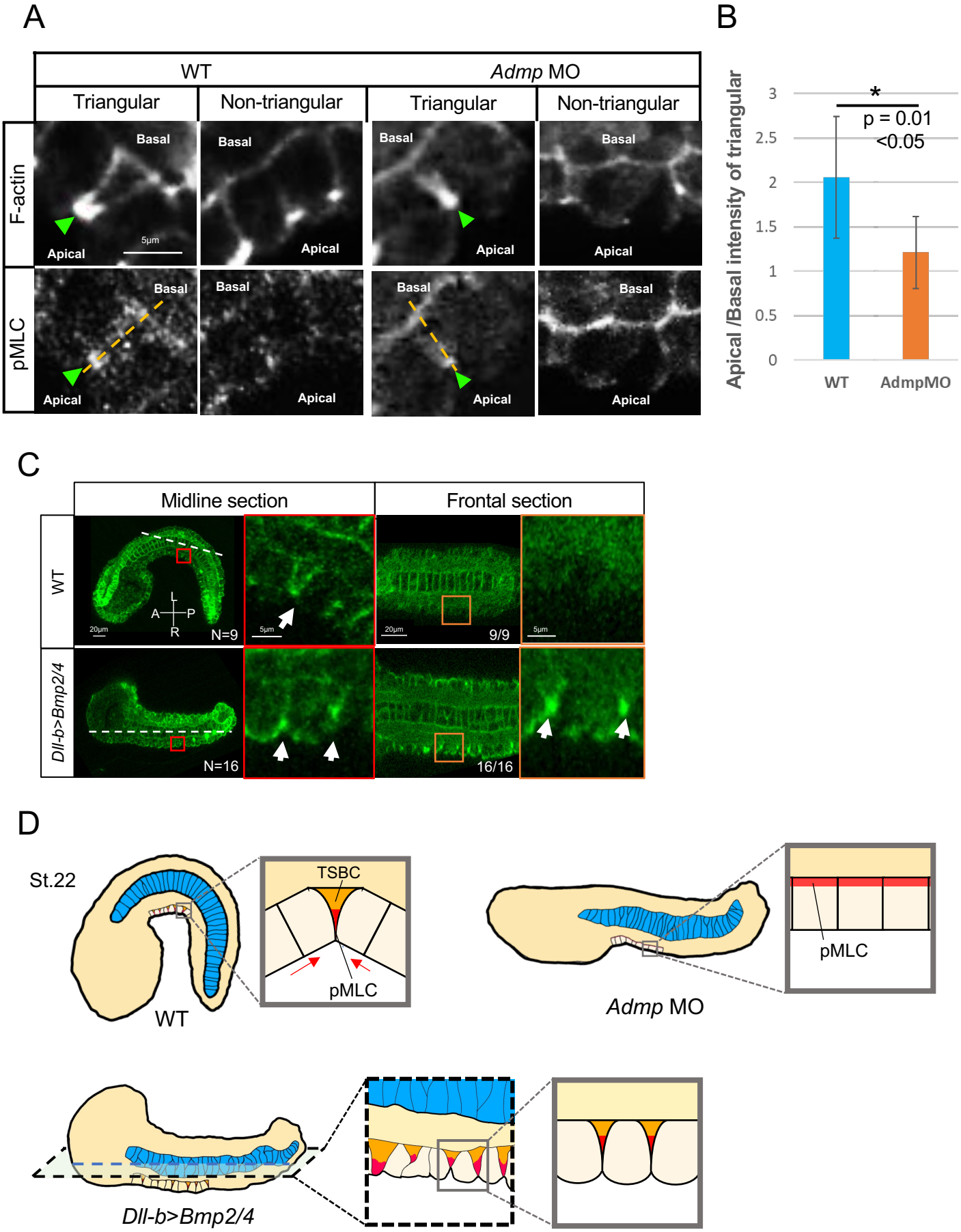
A
WT
Admp MO
Triangular
Non-triangular
Triangular
Non-triangular
F-actin
pMLC
Basal
Apical
5μm
B
Apical /Basal intensity of triangular
3
2.5
2
1.5
1
0.5
0
*
p = 0.01
<0.05
WT
AdmpMO
C
Midline section
Frontal section
WT
Dll-b>Bmp2/4
L
A
P
R
20μm
5μm
N=9
9/9
N=16
16/16
D
St.22
TSBC
pMLC
WT
Admp MO
Dll-b>Bmp2/4

Fig. 4

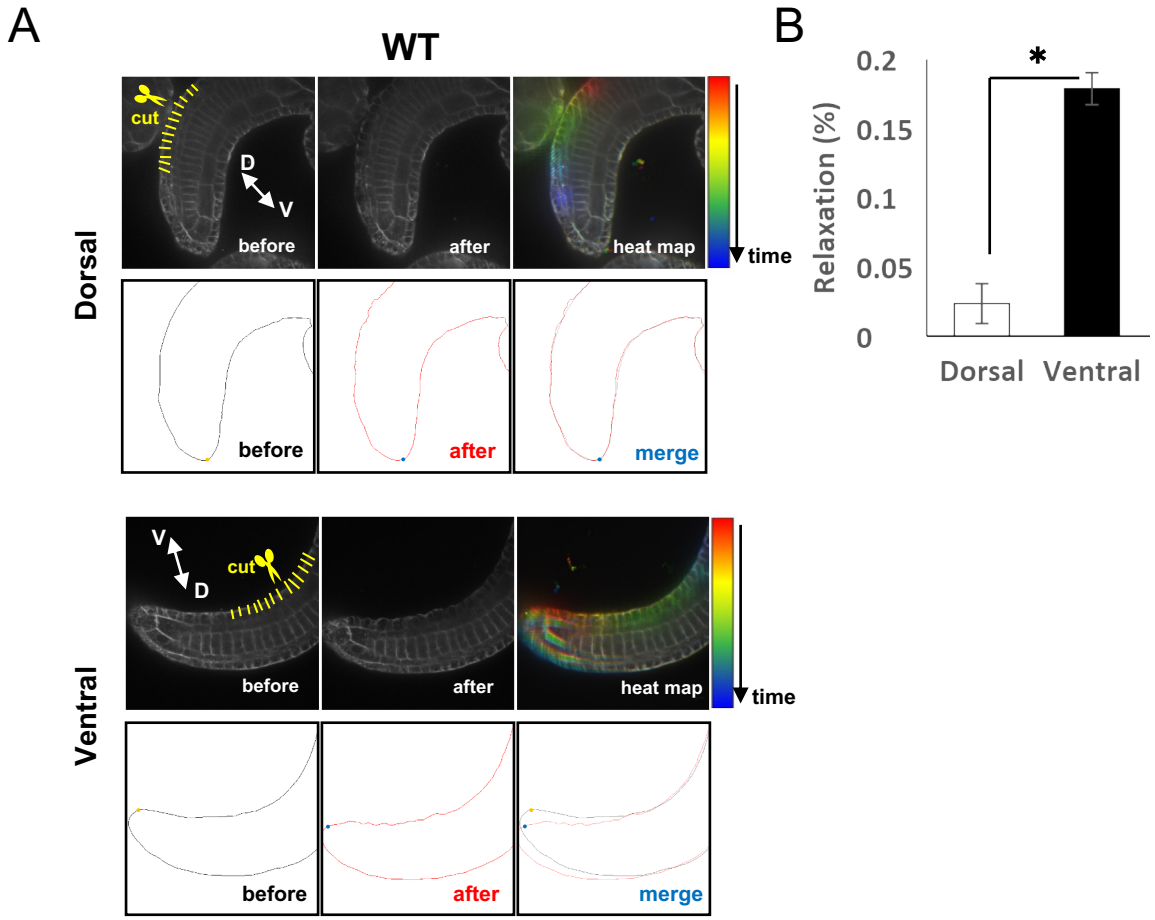
A
WT
Dorsal
cut
D
V
before
after
heat map
time
before
after
merge
Ventral
V
D
cut
before
after
heat map
time
before
after
merge
B
Relaxation (%)
0.2
0.15
0.1
0.05
0
*
Dorsal
Ventral

Fig. 5

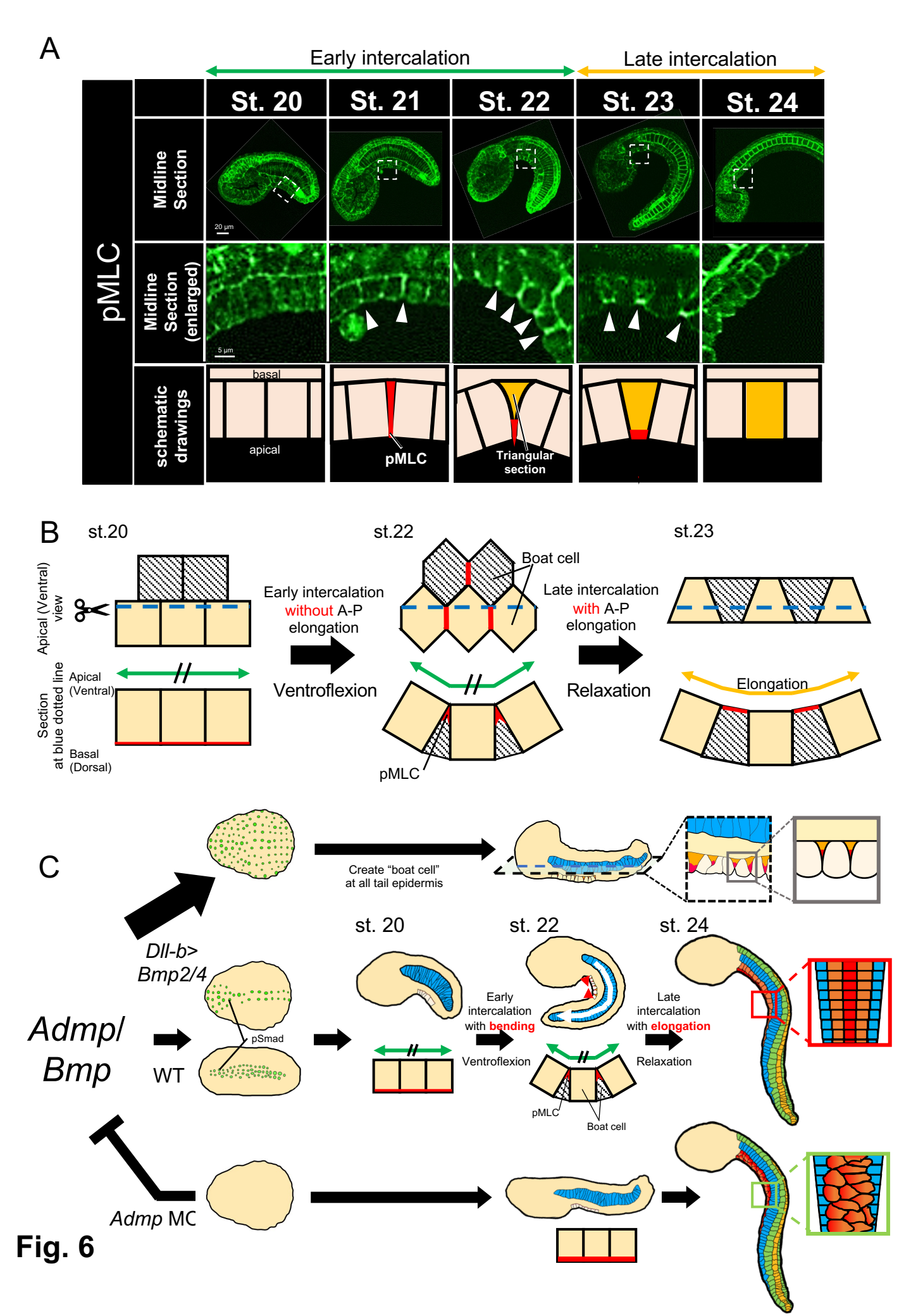
A
Early intercalation
Late intercalation
St. 20
St. 21
St. 22
St. 23
St. 24
pMLC
Midline Section
Midline Section (enlarged)
schematic drawings
20 µm
5 µm
basal
apical
pMLC
Triangular section
B
st.20
st.22
st.23
Apical (Ventral) view
Section at blue dotted line
Apical (Ventral)
Basal (Dorsal)
Early intercalation without A-P elongation
Ventroflexion
Boat cell
pMLC
Late intercalation with A-P elongation
Relaxation
Elongation
C
Create "boat cell" at all tail epidermis
Dll-b> Bmp2/4
Admp/ Bmp
WT
pSmad
st. 20
st. 22
st. 24
Early intercalation with bending
Ventroflexion
pMLC
Boat cell
Late intercalation with elongation
Relaxation
Admp MC

Fig. 6